Electronic Supplementary Information (ESI)

Realizing the Potential of Hydrophobic Crystalline Carbon as a Support for Oxygen Evolution Electrocatalysts

Myeong-Geun Kim,[a,†] Tae Kyung Lee,[a,b,†] Eungjun Lee,[a,c,†] Subin Park,[a] Hyun Ju Lee,[d] Haneul Jin,[e] Dong Wook Lee,[a] Min-Gi Jeong,[f] Hun-Gi Jung,[f] Kyungmin Im,[a] Chuan Hu,[g] Hyung Chul Ham,[d] Kwang Ho Song,[b] Yung-Eun Sung,[c,h] Young Moo Lee,[g] and Sung Jong Yoo[a,i,j,‡]*

[a]Center for Hydrogen·Fuel Cell Research, Korea Institute of Science and Technology (KIST), 5 Hwarang–ro 14–gil, Seongbuk–gu, Seoul 02792, Republic of Korea

[b]Department of Chemical and Biological Engineering, Korea University, 5–1 Anam–dong, Seongbuk–gu, Seoul 02841, Republic of Korea

[c]School of Chemical and Biological Engineering, Seoul National University, Gwanak–ro, Gwanak–gu, Seoul 08826, Republic of Korea

[d]Department of Chemistry and Chemical Engineering, Inha University, 100 Inha–ro, Michuhol–gu, Incheon 22212, Republic of Korea

[e]Department of Energy and Materials Engineering, Dongguk University–Seoul, Seoul 04620, Republic of Korea

[f]Energy Storage Research Center, Korea Institute of Science and Technology (KIST), 5 Hwarang–ro 14–gil, Seongbuk–gu, Seoul 02792, Republic of Korea

[g]Department of Energy Engineering, College of Engineering, Hanyang University, 222 Wangsimni–ro, Seongdong–gu, Seoul 04763, Republic of Korea

[h]Center for Nanoparticle Research, Institute for Basic Science (IBS), Gwanak–ro, Gwanak–gu, Seoul 08826, Republic of Korea

[i]Division of Energy & Environment Technology, KIST School, University of Science and Technology (UST), 217 Gajeong–ro, Yuseong–gu, Daejeon 34113, Republic of Korea

[j]KHU–KIST Department of Converging Science and Technology, Kyung Hee University, 26 Kyungheedae–ro, Dongdaemun–gu, Seoul 02447, Republic of Korea

*Corresponding Author: Sung Jong Yoo; Tel: +82–2–958–5260; E–mail: ysj@kist.re.kr

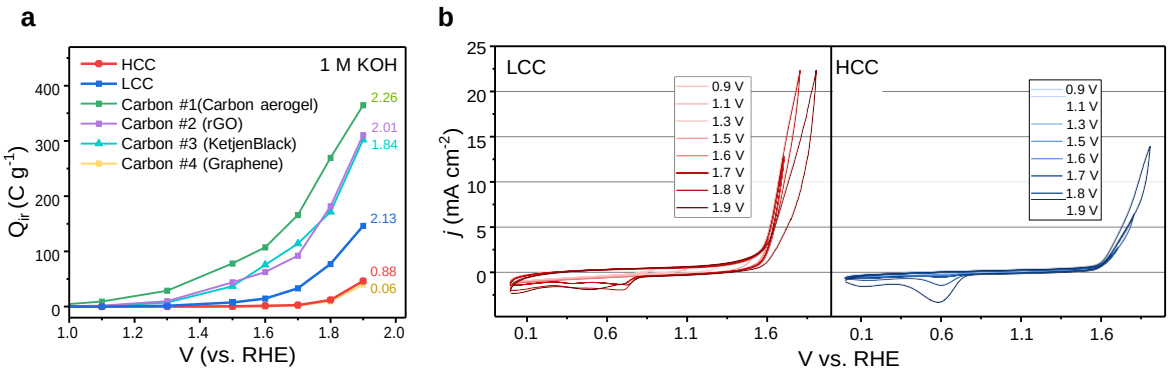

Figure S1. (a) Irreversible charge (Q_{ir}) test results for various carbons in 1 M KOH. The numbers written next to each graph represent the I_D/I_G ratio values obtained from Raman spectroscopy. (b) CV spectra for LCC and HCC obtained by cycling from 0 to the specified voltage, respectively.

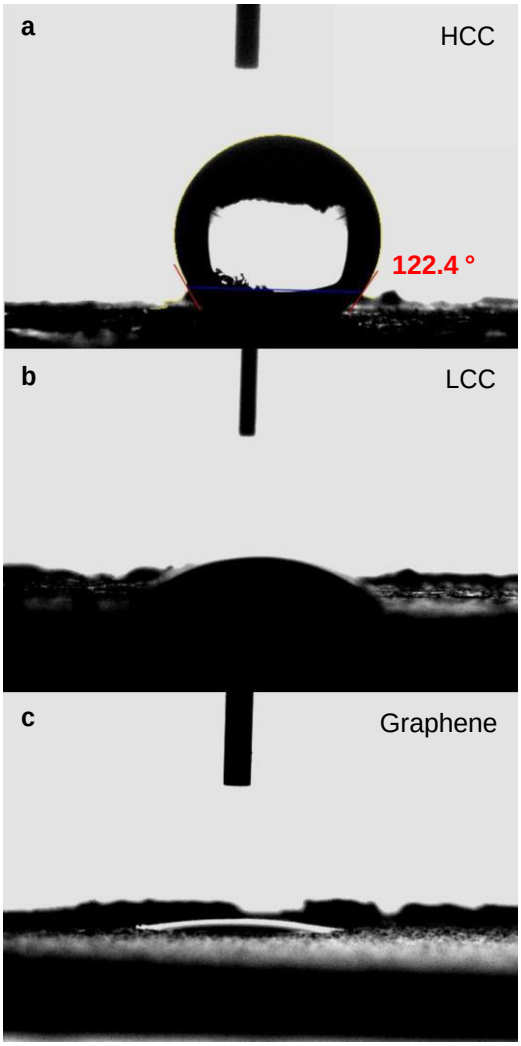

Figure S2. Contact angle measurements of water droplet on (a) HCC, (b) LCC, and (c) graphene, respectively.

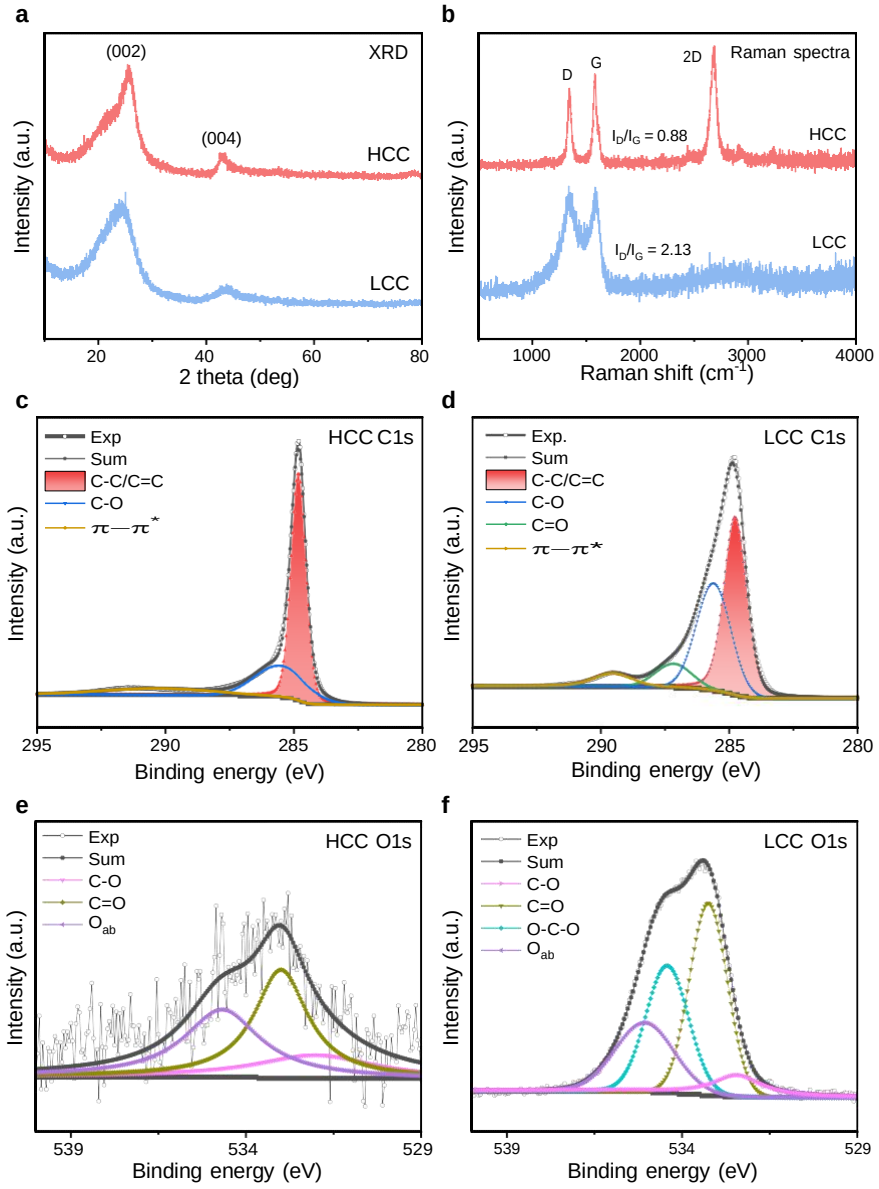

Figure S3. Structural and chemical analysis of HCC and LCC: (a) XRD patterns, (b) Raman spectra, and XPS spectra for (c, d) C 1*s* and (e, f) O 1*s*, respectively.

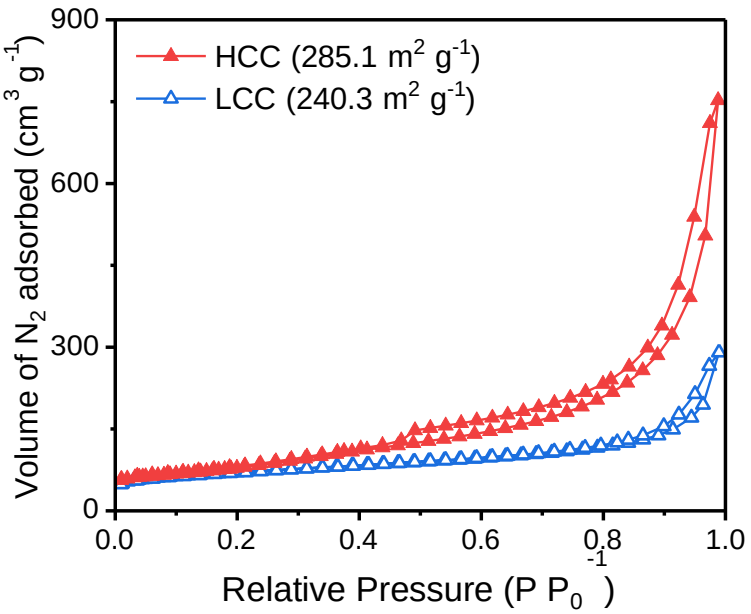

Figure S4. BET surface area plots for HCC and LCC, respectively.

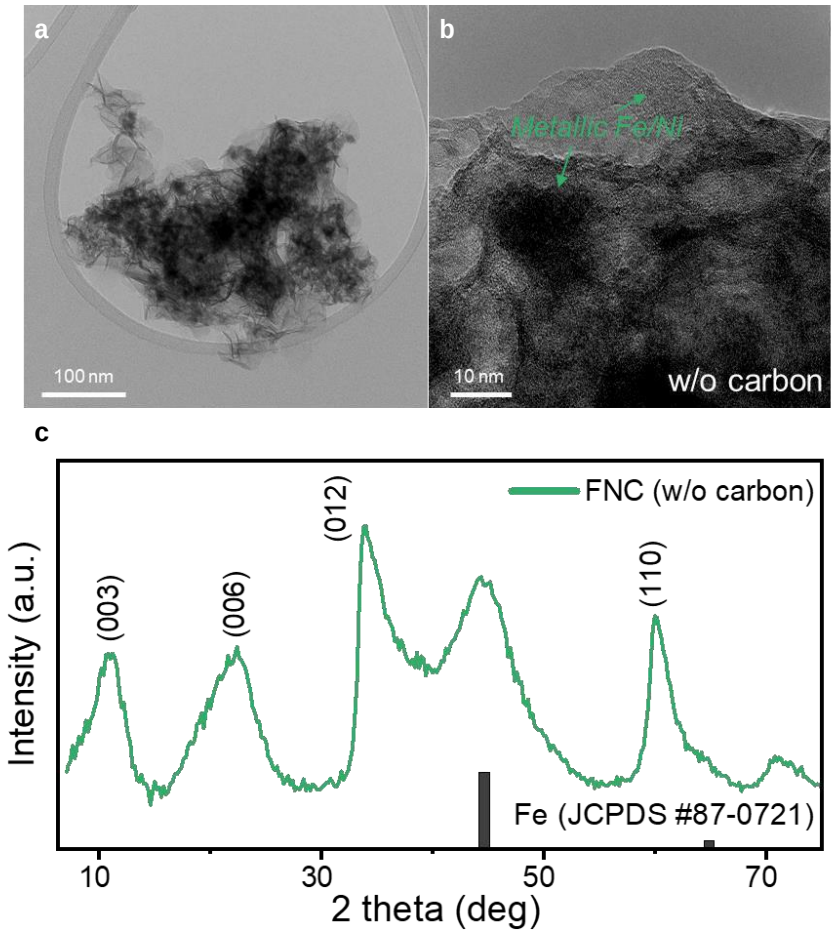

Figure S5. (a, b) TEM images and (c) XRD pattern of FNC obtained in the absence of carbon supports with reference pattern of Fe.

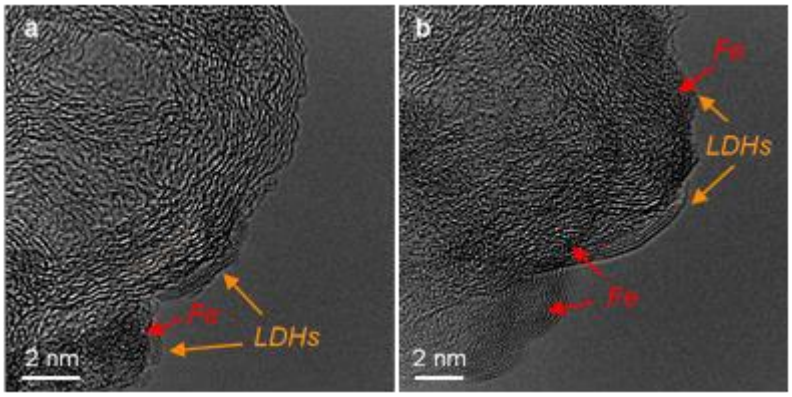

Figure S6. (a, b) TEM images of FNC/HCC obtained at reaction time of 3 min.

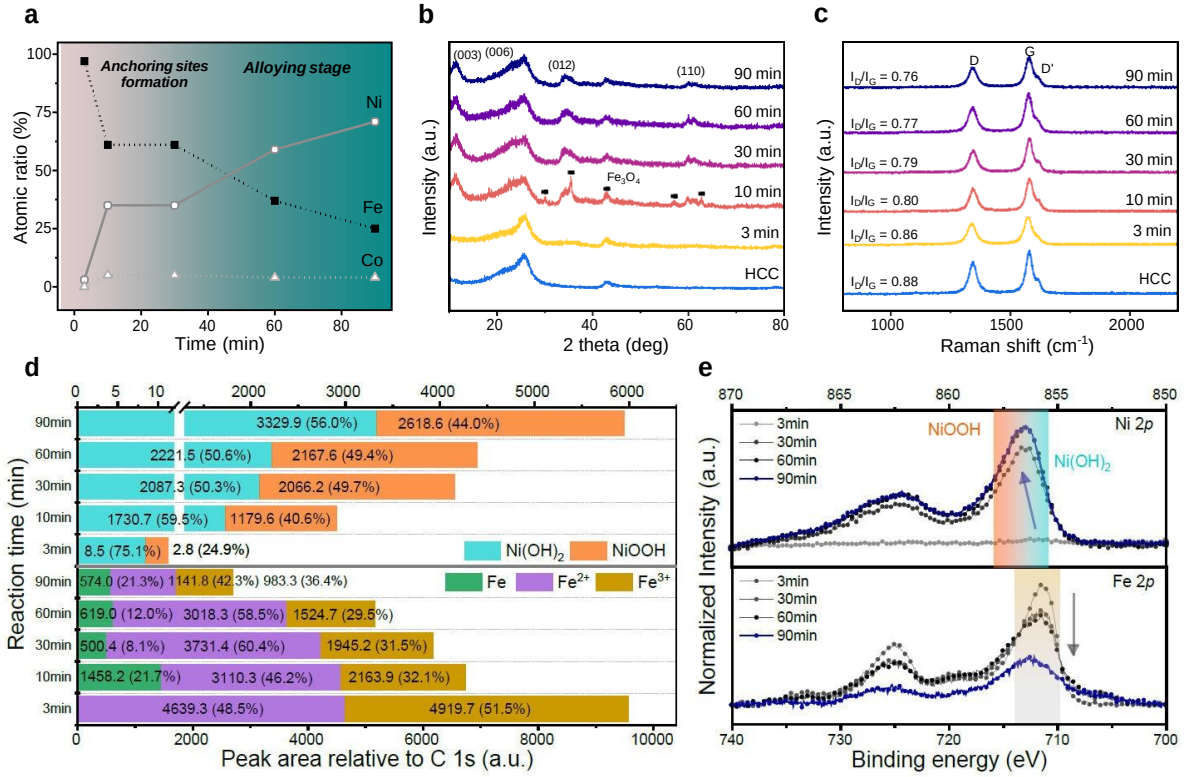

Figure S7. Time-dependent *ex-situ* characterization of FNC/HCC; (a) EDS atomic ratio of Fe, Ni, and Co. (b) XRD patterns. (c) Raman spectra. (d) Changes in oxidation states of Fe and Ni and (e) corresponding XPS spectra for Ni 2*p* and Fe 2*p* during FNC/HCC synthesis.

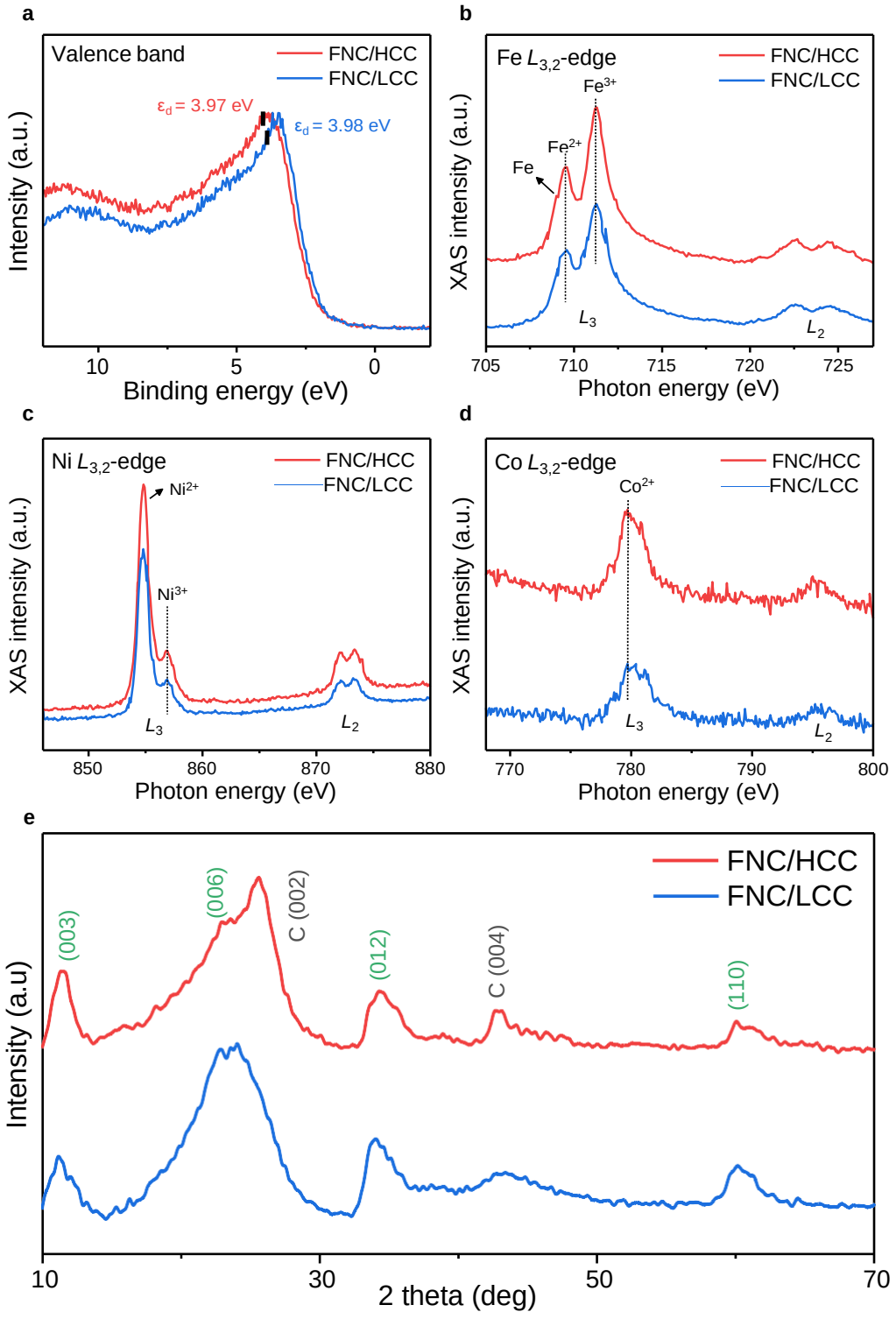

Figure S8. XPS spectra for (a) valence band region. Near edge X-ray absorption fine structure spectra for (b) Fe $L_{3,2}$-edge, (c) Ni $L_{3,2}$-edge, and (d) Co $L_{3,2}$-edge of FNC/HCC and FNC/LCC. (e) XRD patterns for FNC/HCC and FNC/LCC.

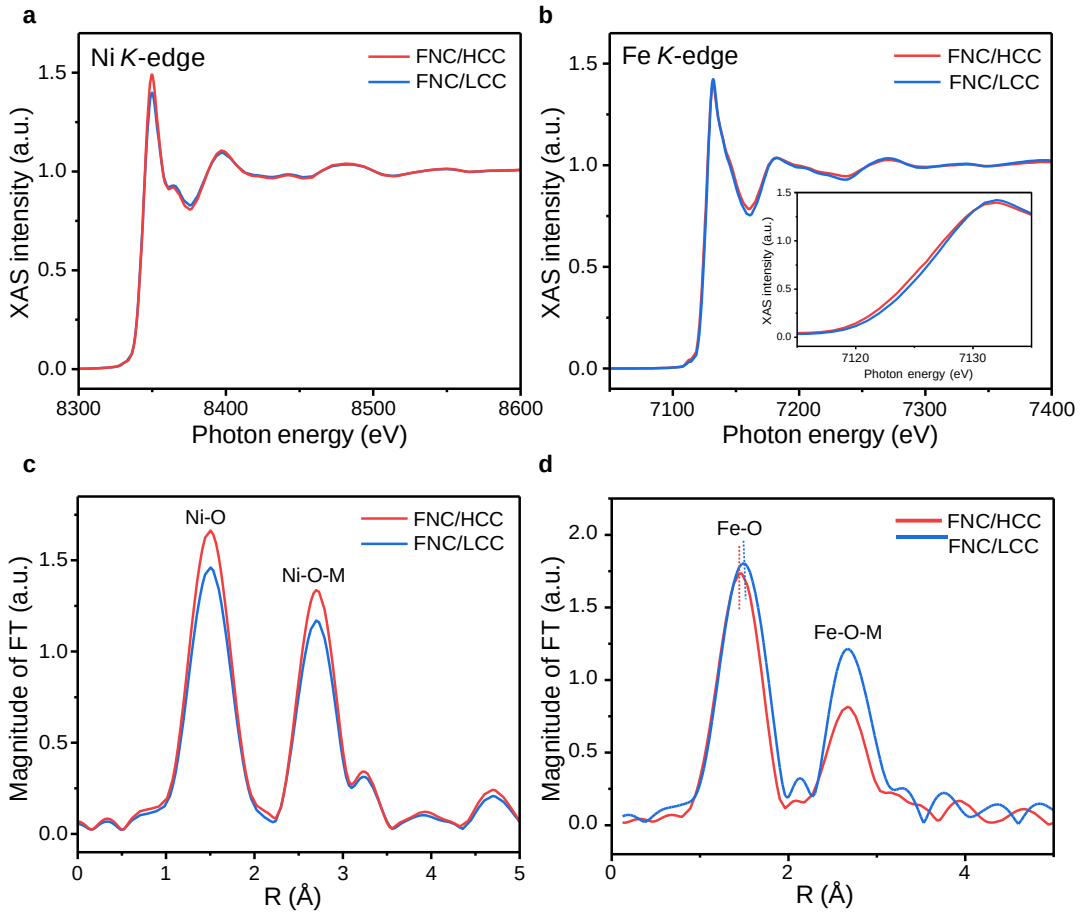

Figure S9. X-ray absorption spectroscopy results of FNC/HCC and FNC/LCC. (a) Ni *K*-edge and (b) Fe *K*-edge X-ray absorption near edge structure spectra and corresponding the FT of extended *X*-ray absorption fine structure spectra of (c) Ni *K*-edge and (d) Fe *K*-edge.

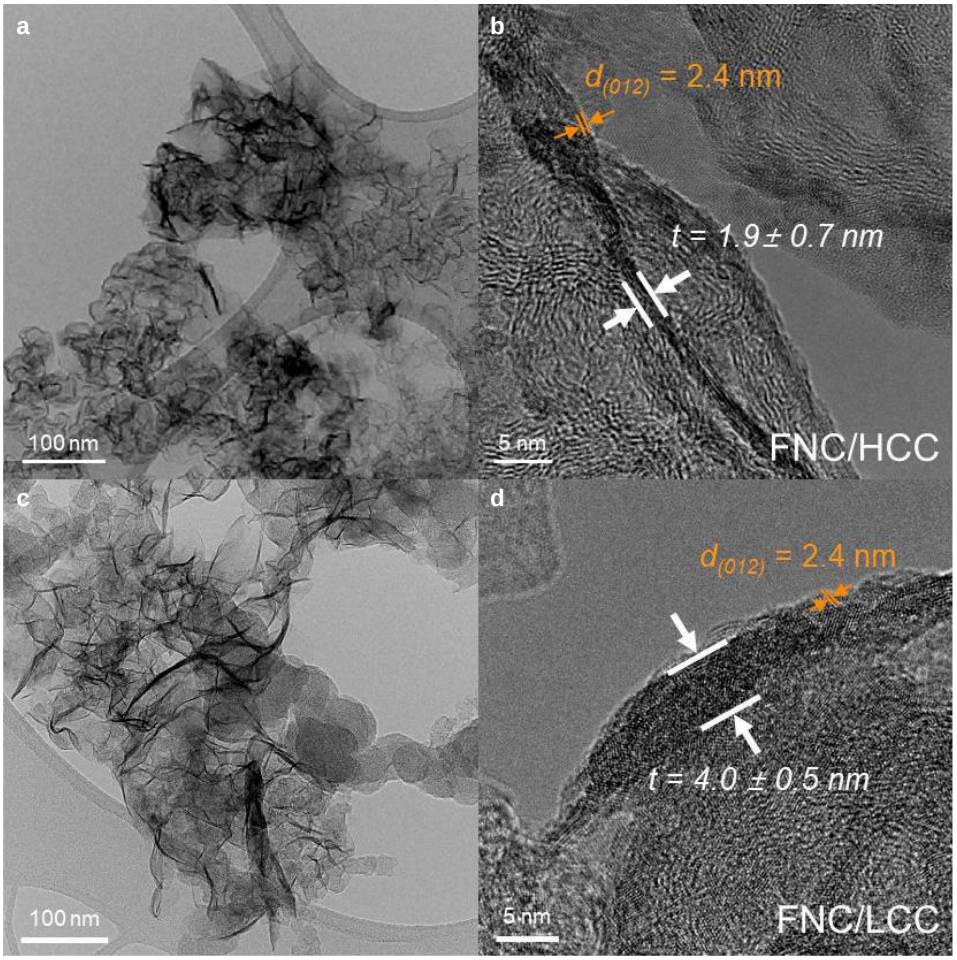

Figure S10. TEM, high resolution TEM images of (a, b) FNC/HCC and (c, d) FNC/LCC, respectively.

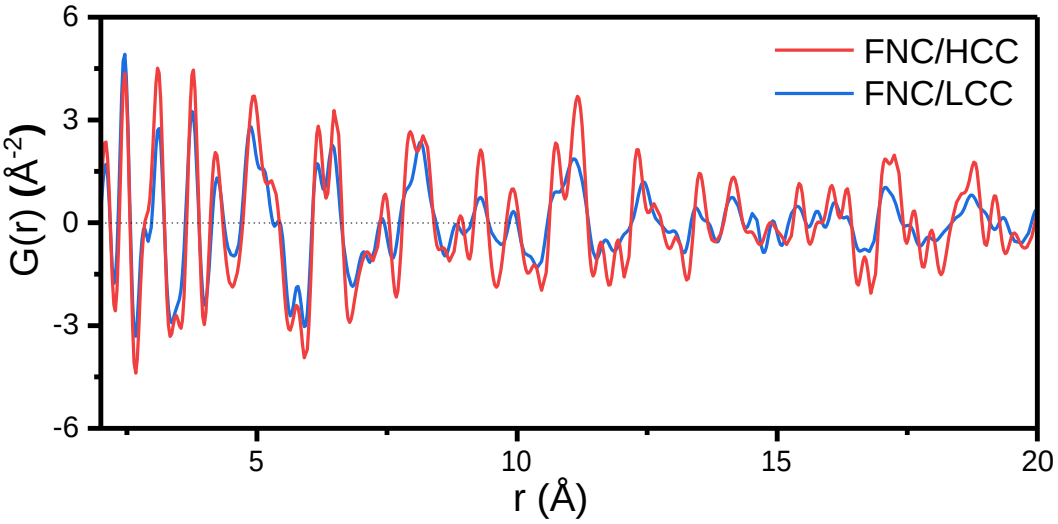

Figure S11. X-ray pair distribution functions for FNC/HCC and FNC/LCC.

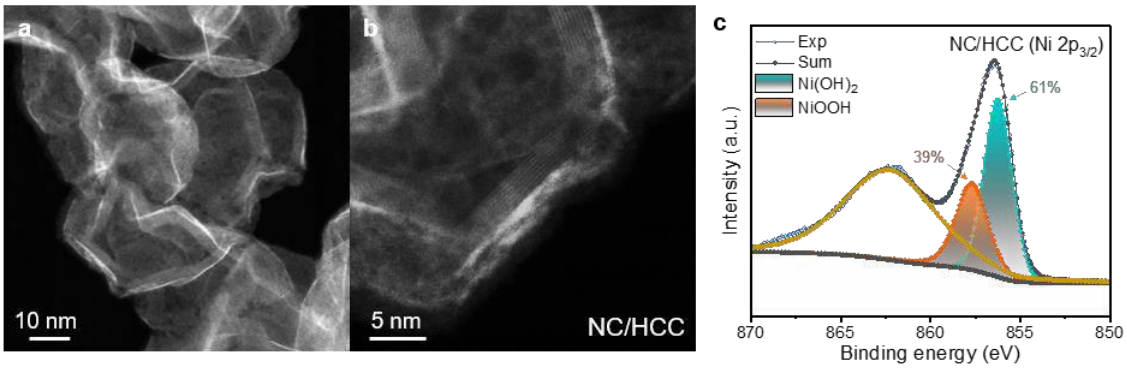

Figure S12 (a, b) STEM images and (c) XPS Ni 2*p* spectrum for NC/HCC obtained without Fe.

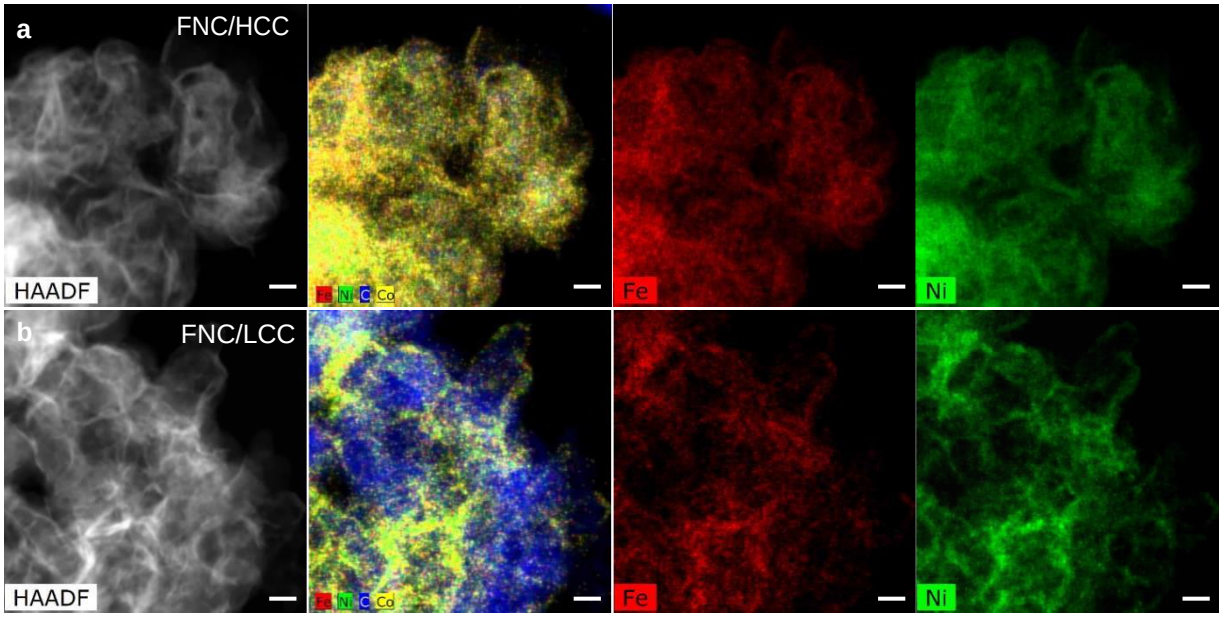

Figure S13. EDS elemental mapping images of (a) FNC/HCC and (b) FNC/LCC obtained after 1000 h and 100 h of reaction, respectively. High angle annular dark field-STEM and overlay image of Fe (red), and Ni (green), Co (yellow), and C (blue).

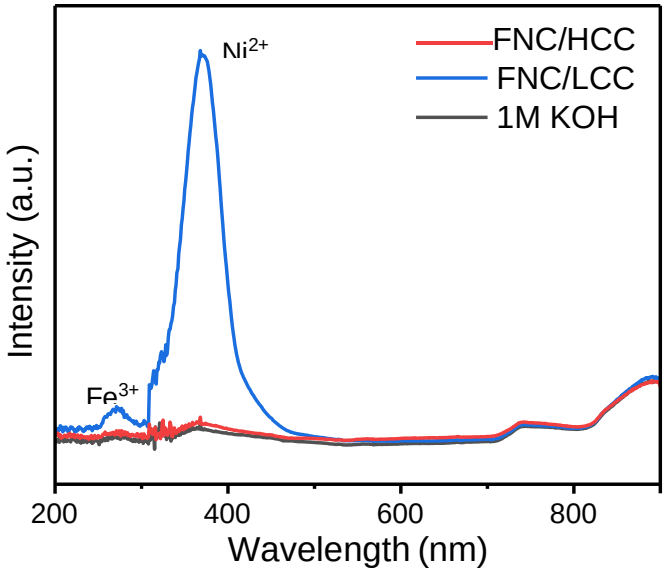

Figure S14. UV-vis absorption spectra of electrolyte collected after stability test. The test were conducted for 100 h and 1000 h with FNC/LCC and FNC/HCC, respectively.

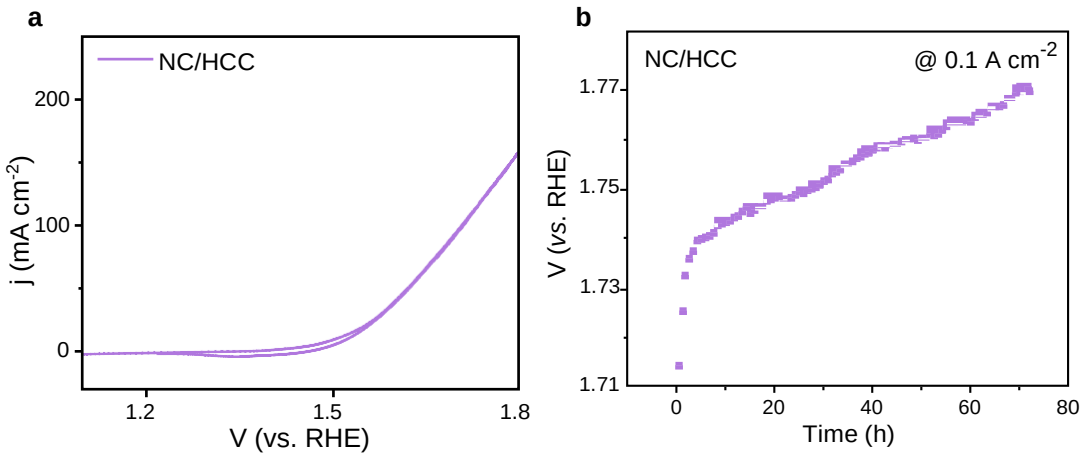

Figure S15. (a) Linear sweep voltammetry curve obtained with NC/HCC. (b) Stability test result under galvanostatic conditions of 0.1 A cm^{-2} at 25℃.

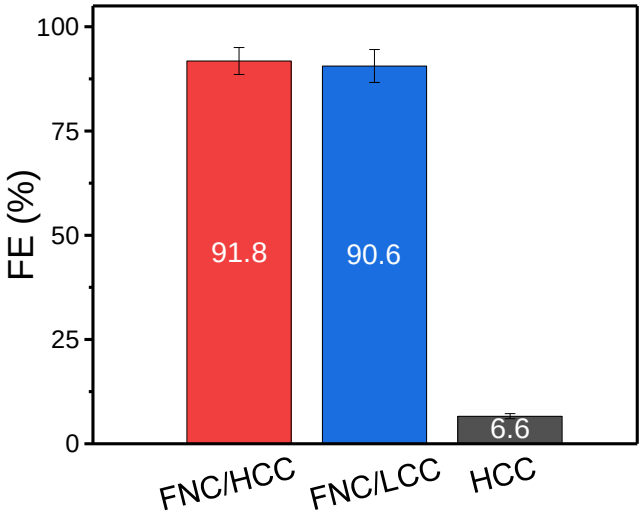

Figure S16. Faradaic efficiency of oxygen evolution for FNC/HCC, FNC/LCC, and HCC. The error bars represent the standard deviations of three independent measurements.

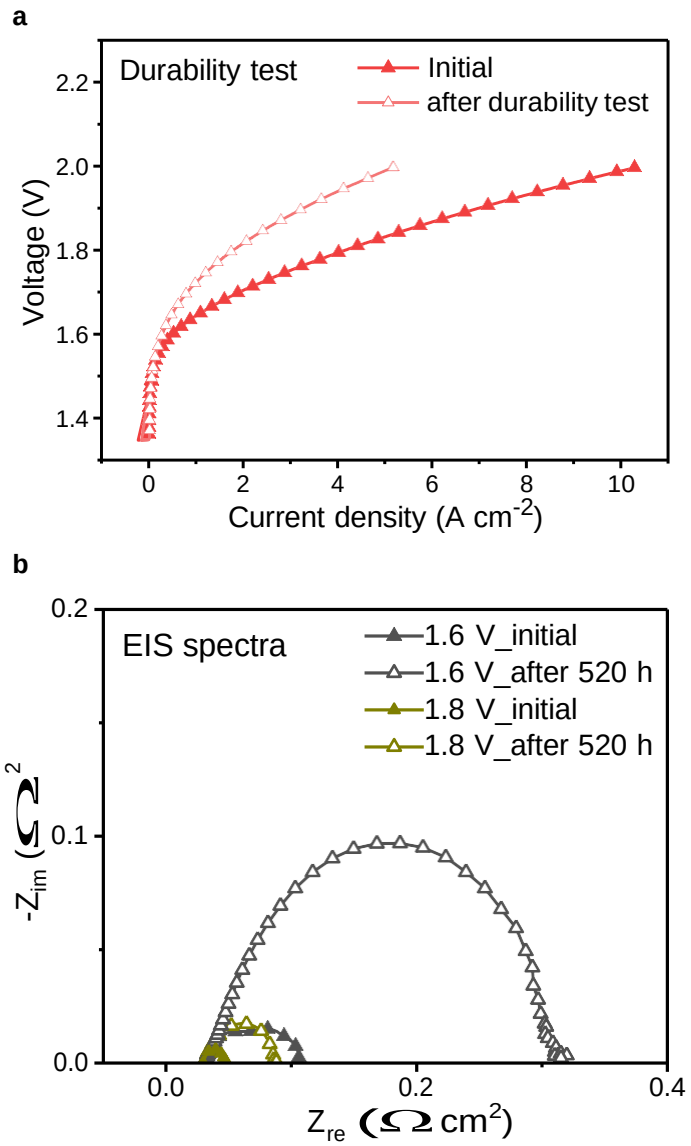

Figure S17. (a) AEMWE performance and (b) EIS spectra for FNC/HCC measured before and after 520 hours of durability test.

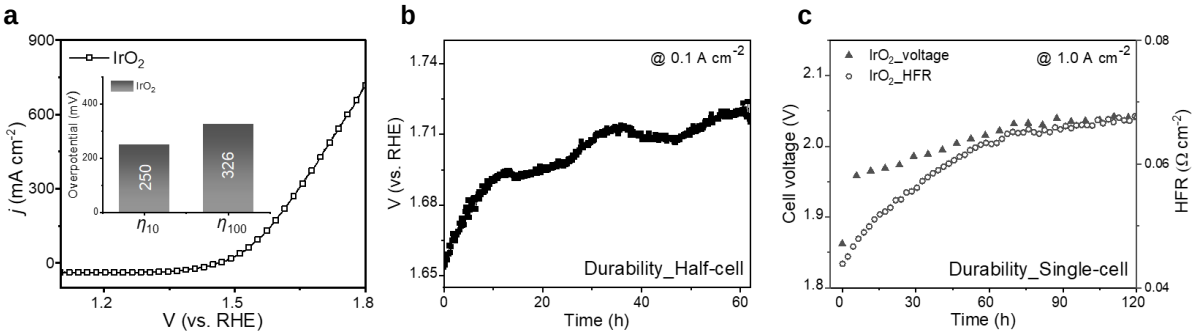

Figure S18. (a) LSV curve for IrO_2 with the inset showing the overpotential for current densities of 10 and 100 mA cm^{-2}. (b) Long-term stability test under galvanostatic conditions of 0.1 A cm^{-2} at 25 °C. (c) AEMWE durability at 1.0 A cm^{-2}.

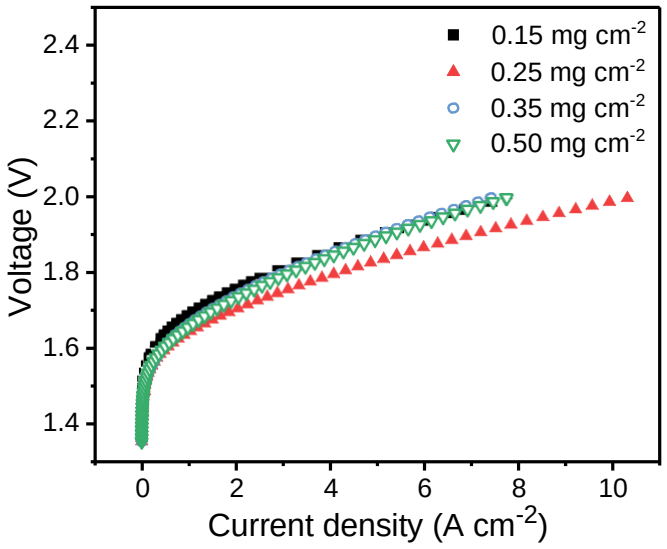

Figure S19. Current–voltage (I–V) curves obtained from different loading mass of FNC electrocatalyst. During MEA fabrication, if the loading amount exceeded 0.50 mg cm^{-2}, the catalysts became detached from the membrane.

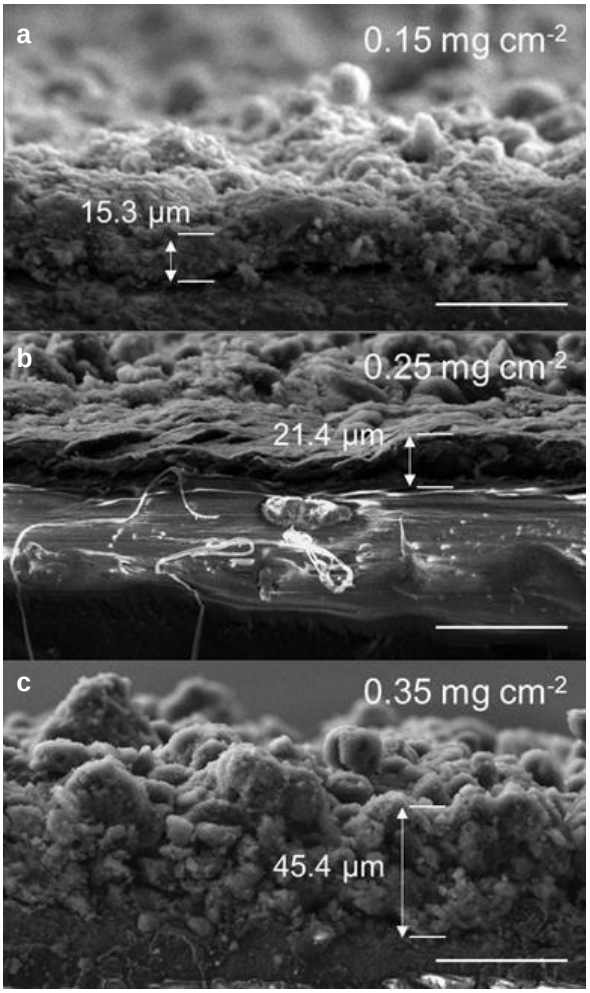

Figure S20. Cross-sectional SEM images of the catalyst layer with different loading mass: (a) 0.15, (b) 0.25, and (c) 0.35 mg cm^{-2}. All scale bars are 50 μm.

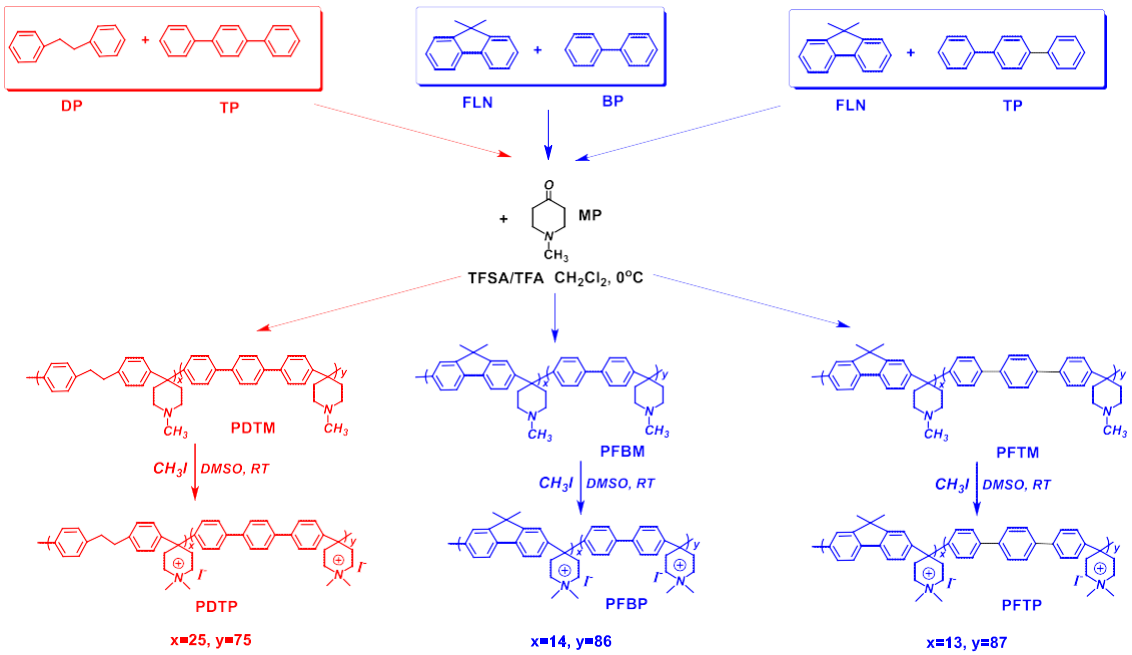

Figure S21. Chemical structure and synthesis routes of PDTP, PFBP, and PFTP.

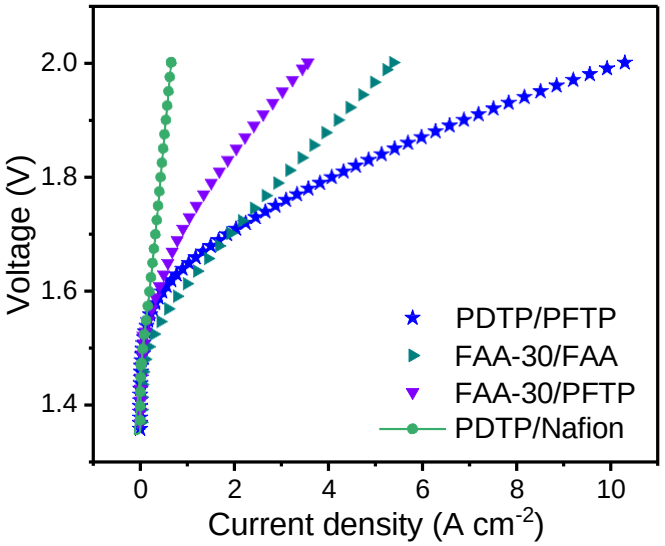

Figure S22. I–V curves obtained using various membrane/anode-ionomer combinations.

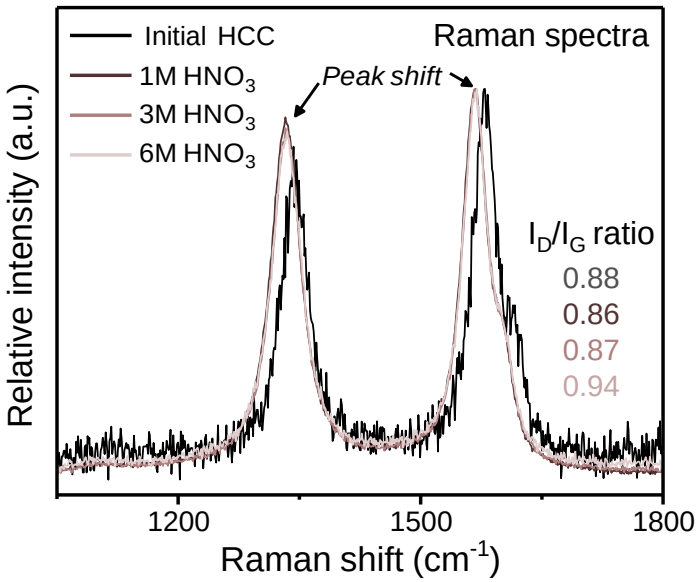

Figure S23. Raman spectra for HCC and acid-treated HCC. I_D/I_G ratio values were obtained from Raman analysis.

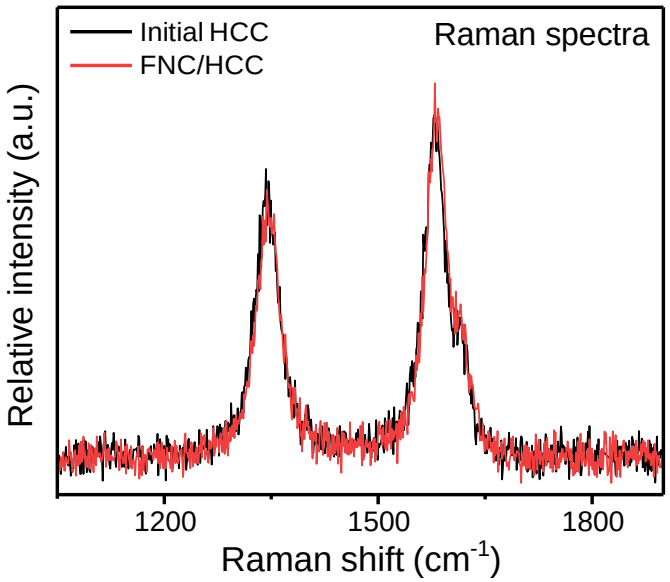

Figure S24. Raman spectra for as-prepared HCC (black) and FNC/HCC (red).

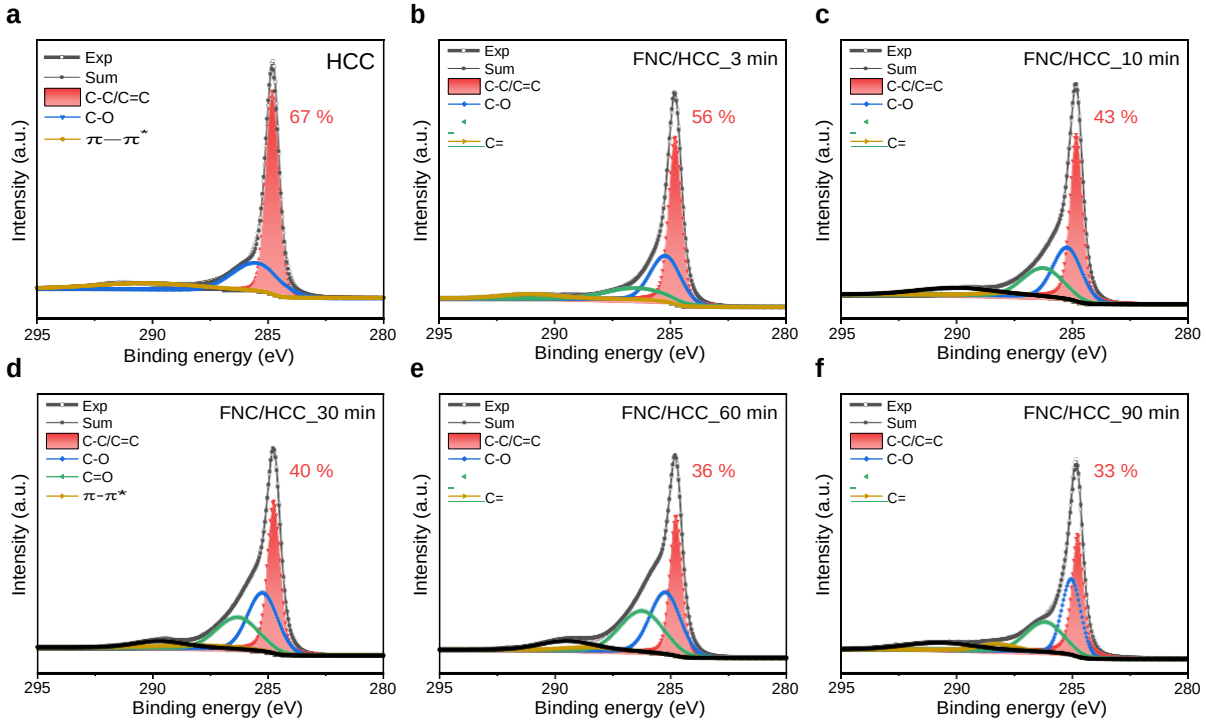

Figure S25. XPS C 1*s* spectra obtained at different stages of FNC/HCC formation: (a) before and after (b) 3 min, (c) 10 min, (d) 30 min, (e) 60 min, and (f) 90 min of the reaction.

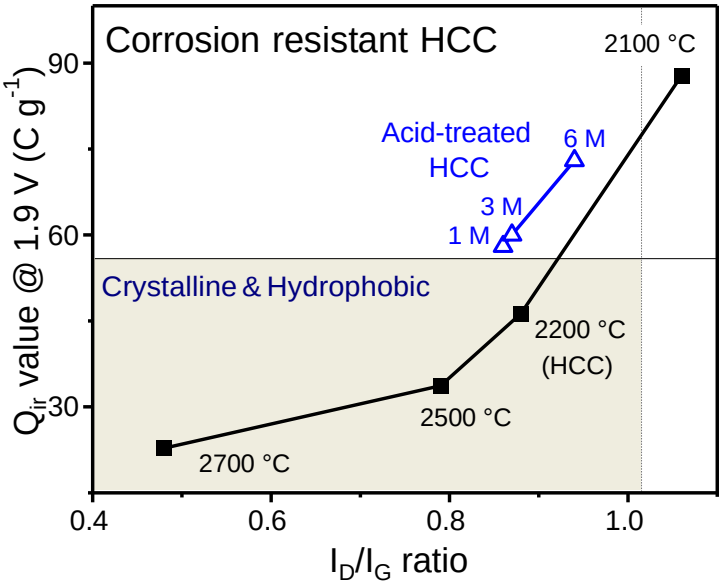

Figure S26. Correlation between I_D/I_G ratio and corrosion resistivity of carbon annealed at different temperatures (2100, 2200, 2500, and 2700 °C) or treated with different concentration (1 M, 3 M, and 6 M) of HNO_3.

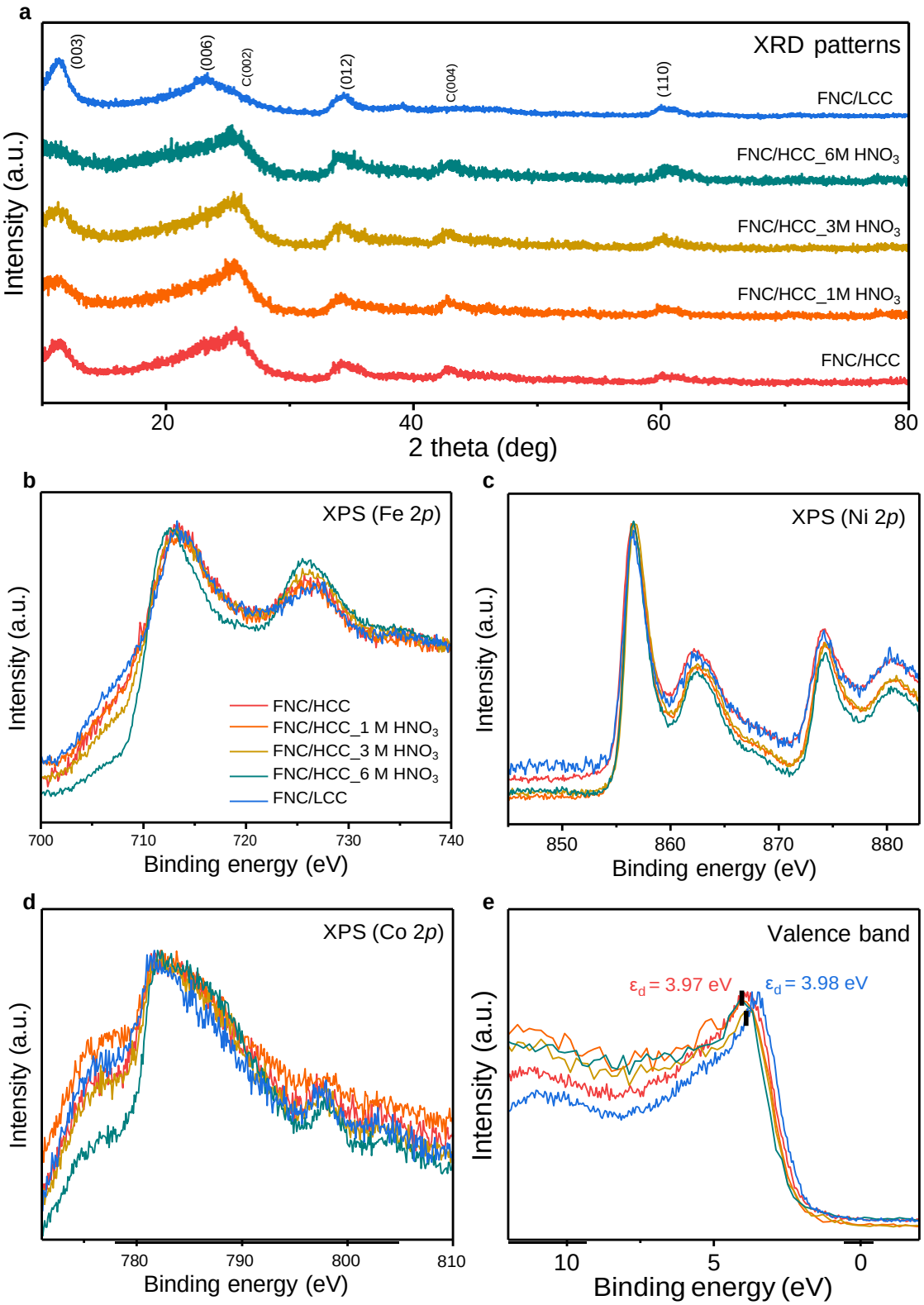

Figure S27. (a) XRD and XPS spectra for (b) Fe 2*p*, (c) Ni 2*p*, (d) Co 2*p*, and (e) valence band of FNC electrocatalyst supported on HCC, acid-treated HCC, and LCC.

ICP-MS	Fe (wt.%)	Ni (wt.%)	Co (wt.%)	Total (wt.%)
FNC/HCC	4.87	14.09	0.40	19.36
FNC/LCC	2.60	10.26	0.40	13.26

Table S1. Comparison of catalyst composition of FNC/HCC and FNC/LCC, determined by ICP-MS.

	FNC/HCC	FNC/LCC	Unsupported FNC
2 theta (degree)	11.48	11.36	10.77
	23.59	22.63	21.96
Crystallite size (nm)	6.81	4.97	2.60
	1.32	1.55	1.63
Interlayer distance (Å)	7.70	7.78	8.21
	3.77	3.93	4.05
Lattice parameter c (Å)	23.11	23.34	24.63
	22.61	23.55	24.27
(006)/(003) plane height ratio	1.05	2.67	1.70

Table S2. Two theta value, crystallite size, interlayer distance, lattice parameter c, and ratio of (006) to (003) obtained from XRD data.

ICP-MS	Fe (at.%)	Ni (at.%)	Co (at.%)
FNC/HCC	25	71	4
After 1000h	18	79	3
FNC/LCC	20	77	3
After 100h	22	76	2

Table S3. Components of the electrocatalysts before and after the stability test determined by the ICP-MS.

Electrocatalyst	*j* @ 1.8 V (A cm^{-2})	Specific power @1.8 V (kW g_{metal}^{-1})	Reference
FNC/HCC	**4.07**	**24.11**	***This work***
FNC/LCC	**2.80**	**16.58**	
IrO_x	3.57	21.14	
	3.5	2.59	*Energy Environ. Sci*., **2021**, *14*, 6338-6348.
Carbon-supported	1.5	0.74	*ACS Appl. Mater. Interfaces*, **2021**, *13*, 37179-37186
	1.0	2.96	*Electrochim. Acta* **2020**, *353*, 136521.
	0.8	0.03	*Electrochim. Acta* **2022**, *413*, 140078.
	0.03	0.49	*J. Mater. Chem. A*, **2021**, *9*, 14043-14051.
	1.0	8.23	*J. Power Sources* **2019**, *415*, 136-144.
	1.6	1.18	*J. Ind. Eng. Chem.* **2022**, *109,* 453–460.
Directed-coated electrocatalysts	2.5	4.50	*ACS Catal*. **2022**, *12*, 135−145.
	1.5	0.74	*ACS Appl. Mater. Interfaces*, **2021**, *13*, 37179-37186
	0.6	0.05	*Energy Environ. Sci.,* **2021**, *14*, 6338.
Oxide-based	1.5	0.54	*Adv. Mater. Interfaces*, **2022**, *9*, 2102063
	1.3	0.19	*J. Mater. Chem. A*, **2020**, *8*, 4290-4299.
	1.0	0.06	*ACS Sustainable Chem. Eng.*, **2020**, *8*, 2344-2349.
	0.63	0.93	*Nat. Energy*, **2019**, *2*, 763-772.
	0.55	0.23	*J. Power Sources* **2021,** *514*, 230563.
	0.15	0.07	*Adv. Funct. Mater.*, **2018**, *28*, 1804355.
	0.10	0.01	*Int. J. Hydrog. Energy*, **2018**, *43,* 21999-22011
	0.025	0.09	*J. Power Source*, **2021**, *485*, 229217

Table S4. AEMWE performance comparison of the state-of-the-arts electrocatalysts.